J Mater Sci: Mater Med (2007) 18:1817–1824
DOI 10.1007/s10856-007-3028-3

Development of graded hydroxyapatite/$CaCO_3$ composite structures for bone ingrowth

F. Heilmann · O. C. Standard · F. A. Müller · M. Hoffman

Received: 15 November 2005 / Accepted: 1 May 2006 / Published online: 5 May 2007

Abstract Ceramic composites composed of constituents with different bone cell reactions present an interesting consideration for a new bone replacement material. The first component of the composite used in this study, hydroxyapatite, is known to be replaced by natural tissue significantly slower than the second, calcium carbonate, which has limited structural stability. A graded hydroxyapatite/calcium carbonate composite with bimodal component distribution was developed using a combined slip infiltration and dip-coating technique from a porous polyurethane sponge replica. A graded hydroxyapatite scaffold with porosities from 5 to 90% was produced and then infiltrated with a calcium carbonate slip and sintered. The resultant composite had improved mechanical properties compared with the monolith as measured by crushing and moduli tests.

Introduction

Macroporous ceramics have been widely discussed as bone replacement materials in recent years as they have been proven to enable good bone tissue ingrowth behavior [1]. A focus of this research is to synthetically reconstruct the natural porosity distribution in human bone. Calcium phosphate ceramics, especially hydroxyapatite $Ca_{10}(PO_4)_6(OH)_2$, form the basis for much of this work due to their compatibility with human bone [2]. One approach to improve the mechanical properties of porous constructs, whilst maintaining cellular and tissue ingrowth, is to functionally grade the porosity, i.e. to have a high porosity in the outer part of the implant to enable cell ingrowth and a core with lower porosity for mechanical stability, with gradient changes between both extremes [3, 4]. Bone itself shows a bimodal distribution of cancellous and compact parts, which fulfill different purposes in the human body [5].

In general, it is difficult to create porous ceramic scaffolds covering the full range of graded porosity using one single technique. Foaming or dip-coating to coat the surface of ligaments of pyrolysable foams are examples of replica methods which are, for the most part, suitable for porosities above 50% [6]. Conversely, full infiltration of sacrificial templates, such as foams, has been used to produce porosities below 50% [7]. In this paper, both infiltration and dip-coating techniques are combined to create low and high porosities in one single ceramic body with a bimodal distribution by a combined polyurethane sponge infiltration and dip-coating procedure.

The extremely poor structural strength of highly porous scaffolds means that usually they are not suitable for implantation. However, it has been shown that the infiltration of a second phase can significantly improve the strength of a porous body, even if the second phase is itself structurally weak [7]. Hence, a temporary filler is needed to provide sufficient strength for handling and initial use. Furthermore, this filler should be bioresorbable, giving room for the ingrowth of natural bone into the hydroxyapatite (HAp) scaffold. Biodegradable polymers such as polylactic acid [8] have, in particular, already been used for

F. Heilmann · F. A. Müller
Department of Materials Science (III)—Biomaterials, University of Erlangen-Nürnberg, Henkestr 91, 91052 Erlangen, Germany

F. Heilmann · O. C. Standard · M. Hoffman (✉)
School of Materials Science and Engineering, University of New South Wales (UNSW), Sydney, NSW 2052, Australia
e-mail: mark.hoffman@unsw.edu.au

similar purposes. In the present work, the designated filling material is calcium carbonate $CaCO_3$, which has proven biodegradability [9]. A major potential advantage compared to polymers is the provision of calcium during decomposition to enhance natural bone formation [10].

This paper describes the development of a hydroxyapatite/calcium carbonate composite, having either constant or layered graded composition, through the use of a polyurethane sponge infiltration and dip-coating process. The polymer foam is used as a template and compressed to different densities before infiltration or dip-coating. The gradient is obtained by stacking different sponge layers followed by a combined dip-coating and infiltration route. The composite is then characterized in terms of its microstructure and mechanical properties.

Material processing and characterization methods

Preparation of porous HAp

Polymer preform preparation

Commercially available polyurethane foam with an average ligament diameter of 55 μm (Bulpren S-28133, Eurofoam, Kremsmünster, Austria) shown in Fig. 1 was used as a template for creating porous ceramic scaffolds. Variations in porosity were obtained via compression of the foam templates based upon an equation first reported by Cichocki et al. [3]. Knowing the initial volume fraction of the polymer foam F_{Pu}^{0} (here 0.025 for polyurethane foam), the desired volume fractions after compression F_{Pu} and Poisson's ratio for the foam v_{sponge} (here 0.04 for the polyurethane foam) [11], the compressive strain ε_{c} can be calculated according to:

$$F_{\mathrm{Pu}} = \frac{F_{\mathrm{Pu}}^{0}}{(1-\varepsilon_{\mathrm{c}})\left(1+v_{\mathrm{sponge}}\varepsilon_{\mathrm{c}}\right)} \tag{1}$$

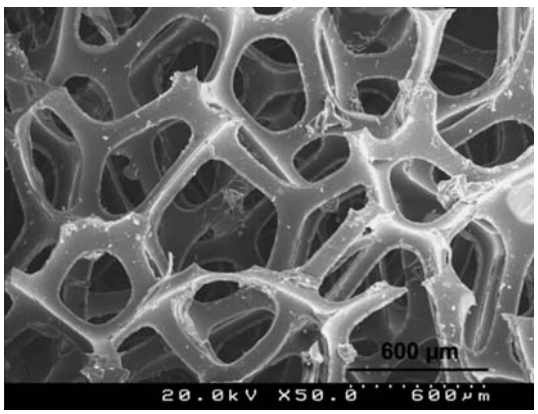

Fig. 1 SEM micrograph of polyurethane foam template

Compression of the polyurethane foam was undertaken in an uniaxial hot press and held at a temperature of 160 °C for 1 h to produce permanent foam compression.

Two types of samples with either constant or graded porosity were prepared. Foam preforms for the constant porosity samples were compressed from varying initial sizes to a height of 4 mm to produce foam template densities of 5–30% in steps of 5%. Graded porosity preforms were constructed by stacking similarly produced 2 mm foam layers, with densities in the order of 5, 10, 15, 20 and 30% density, these then being bonded together by hot pressing under minimal pressure at 160 °C.

Hydroxyapatite slip preparation

An infiltration slip consisting of 25 vol.% HAp powder (Captal R Hydroxylapatite Sintering Grade P218, Plasma Biotal Ltd, Tideswell, UK), 2.125 wt% dispersant (Dispex A40, Ciba Specialty Chemicals Inc., Basel, Switzerland) based on the solids content, 0.18 wt% antifoaming agent (Contraspum KWE, Zschimmer and Schwarz, Lahnstein, Germany), 0.4 wt% wetting agent (Glydol N 109 NEU, Zschimmer and Schwarz, Lahnstein, Germany), and 2.5 wt% binder (Duramax B-1052, Rohm and Haas, Lauterbourg, France) was prepared. A similar slip for dip-coating was prepared; in addition to the components just listed, this slip contained 0.6 wt% of antisedimentation agent (Optapix G-1201, Zschimmer and Schwarz, Lahnstein, Germany) to increase slip viscosity. Concentrated ammonia solution was used to set the pH of both suspensions to 9. A 30 min ultrasonic deagglomeration step followed mixing for all slips.

Infiltration and dip-coating processes

Infiltration was undertaken in an adjustable mould consisting of a gypsum block covered with a porous membrane (Supor-200 from Pall Gelman Sciences, Michigan, USA) to enable water flow but to prevent impurities from the mould entering the specimens. Ungraded compressed foam samples, having individual densities of 5–30% in steps of 5%, were placed on a support membrane and enclosed in perspex blocks which were partially wrapped with teflon tape (PTFE Ebony, J. Blackwoods & Son Ltd., Smithfield, Australia) to prevent sticking. The mould was placed into a laboratory vacuum chamber with the infiltration slip drawn through a tube into the chamber and into the foam. The vacuum was lowered and raised several times to ensure complete infiltration of the foam. To prevent cracking, samples were dried slowly over several days, firstly in a closed container and then in ambient air. A final drying treatment for 10 h at 40 °C followed.

Dip-coating was undertaken for foam templates with 5, 10 and 15% density by immersing the ungraded foam pieces into

the slip optimised for the dip-coating process, then removing the excess by squeezing the foam between two perspex blocks. The same drying step as for the infiltrated samples followed with the samples placed on uncompressed foam pieces to enable airflow from all sides to give uniform drying.

The graded foams were prepared using a combined method of both infiltration and dip-coating. A stack of the 2 mm polymer foam layers with densities in the order 10, 20, 30, 15 and then 5% was dip-coated, squeezed and dried as described above. Then an infiltration step followed. For this, two stacks were placed in an infiltration mould with the 10% foam layers on the bottom and separated by an uncompressed foam piece, adjacent to all layers. The infiltration was undertaken in the vacuum chamber with the slip poured into the uncompressed foam and entering the dip-coated stacks from the 10% density foam template. The amount of slip used ensured that only the layers formed from the 10, 20 and 30% foam were infiltrated. The resultant structure therefore consisted of 10, 20 and 30% infiltrated foam layers and 15 and 5% dip-coated layers.

Polymer burnout and sintering

Separate thermogravimetric analyses (Pyris 1 TGA, Perkin Elmer, Wellesley, US) of the polyurethane and dried binder were done in air using a heating rate of 10 °C/min. Weight loss maxima for the foam occurred at 300, 380 and 430 °C and for the binder at 390 °C. These maxima were used to optimize the pyrolysis and sintering programme. Pyrolysis was undertaken according to the following schedule: heating at 30 °C/h to 350 °C with 2 h hold, then to 410 °C and 1 h hold, then 40 °C/h to 800 °C with 1 h hold, followed by cooling to room temperature at the natural cooling rate of the furnace. Samples were then sintered by heating at 100 °C/h up to 1,250 °C and held for 2 h, and then allowed to cool at the natural cooling rate of the furnace.

Preparation of the HAp/$CaCO_3$ composite

Slip preparation and infiltration

Composites were prepared by infiltrating a calcium carbonate ($CaCO_3$) slip into a porous HAp scaffold. The $CaCO_3$ was a ground natural powder (Omya Australia Pty. Ltd.). EDX elemental analysis (Oxford Isis EDX Analyser, Oxford Instruments PLC, Oxon, UK) of the powder indicated impurity contents of 1.1 ± 0.1 wt% Mg and 0.6 ± 0.4 wt% Si. Particle size analysis (Coulter LS Particle Size Analyser, Beckman Coulter, Fullerton, US) gave a d_{50} value of 50 μm. A 30 vol.% $CaCO_3$ slip was prepared using the same additives as for the dip-coating slip: 0.625 wt% dispersant based on the solids content, 0.18 wt% antifoaming agent, 0.48 wt% wetting agent, and 2.5 wt% of binder. Also, 0.4 wt% antisedimentation agent was used to slow sedimentation of the slip. Prior to infiltration, the sintered HAp scaffold was immersed in an aqueous solution containing 1 wt% wetting agent, which significantly enhanced its wettability. A short drying step at 70 °C followed. Slip infiltration into the hydroxyapatite preforms using the densities listed in chapter 2.1.1 for graded and ungraded samples were undertaken as described above. Dense samples of both hydroxyapatite and $CaCO_3$ were prepared by casting some slip into the empty mould, followed by the drying steps described in chapter 2.1.3.

Sintering

Burnout of the organic additives was undertaken by heating the samples to 500 °C at a rate of 30 °C/h followed by a 1 h hold. When heated in air, $CaCO_3$ decomposes to CaO and CO_2. According to thermogravimetric analysis (TGA) of the $CaCO_3$ powder using the same conditions as those used above, this decomposition commences at 600 °C and reaches a maximum at about 750 °C. A CO_2-atmosphere was used during sintering to minimize decomposition of the $CaCO_3$. An optimum sintering temperature of 850 °C was determined by ascertaining shrinkage and weight loss after sintering samples at different temperatures between 750 and 900 °C. As it is not an oxidation reaction, it is not necessary to clean the furnace completely of remaining oxygen, but to provide sufficient CO_2. Samples were placed in an alumina container and loosely covered with $CaCO_3$ powder then sintered in a tube furnace employing a continuous flow (approximately 100 mL/min) of CO_2. Samples were heated at 100 °C/h to 850 °C followed by a soak for 2 h at this temperature. The linear firing shrinkage of the dense $CaCO_3$ samples was determined by comparing sample dimensions before and after the heat treatment.

Microstructural analysis and porosity measurement

Infiltrated and dip-coated ungraded porous samples, each approximately $2 \times 2 \times 5$ mm^3, were analyzed by X-ray microtomography (microCT, SkyScan-1072, SkyScan, Artselaar, Belgium). A rotation angle of 180° and a rotation step of 0.9° with an exposure time of 1.9 s per image were chosen to create 200 2D images, which were then used to construct a 3D visualization of the samples. From the 3D reconstruction porosity, pore size distribution, mean pore size and specific surface area were calculated using the manufacturer-supplied software. Porosity was also determined using image analysis of scanning electron microscope (SEM) images. These were prepared by first infiltrating the porous scaffolds with epoxy, cutting and polishing a surface to 1 μm diamond paste before gold-coating. Image analysis software was used to calculate the

amount of porosity from the SEM images using area analysis. Macroporosity was determined for the infiltrated and dip-coated samples from four micrographs for each porosity and confirmed subsequently for the graded samples, while microporosity was calculated from both the ligaments of the HAp sintered foam preforms and the dense HAp samples. Grain size of the HAp and $CaCO_3$ was determined using the line intercept method involving the counting of a minimum of 60 grains in two micrographs of each sample.

Crushing strength and moduli

Compressive strength of the HAp and $CaCO_3$ dense materials, ungraded porous HAp scaffolds, and HAp/$CaCO_3$ composites was measured using a uniaxial crushing test. Ten samples (each $5 \times 5 \times 2$ mm^3) of each material were loaded in compression using a mechanical testing machine (Instron 1185, Instron Co., Canton, US.) at a crosshead speed of 0.3 mm/min and the peak load measured.

Young's and shear modulus were measured by an impulse excitation technique as per ASTM C1259–98. The measurement is based on the resonant frequency of the tested sample caused by a mechanical impulse. The resulting vibrations in the material were detected by a microphone and the signal analyzed to determine the resonant frequency (Analyzer 2000, Brownbear Software). Young's modulus E and shear modulus G were then calculated according to the following [12]:

$$E = 0.9465 \left(\frac{mf_f^2}{b}\right)\left(\frac{L^3}{t^3}\right) T_1 \quad (2)$$

$$G = \frac{4Lmf_t^2}{bt}\left[\frac{B}{(1+A)}\right] \quad (3)$$

where m is the mass of the specimen bar (in g), b, L and t are the width, length and thickness of the bar, respectively (in mm); and f_f and f_t the resonant frequencies (in Hz) in flexural and torsional modes, respectively. T_1, A and B are geometry constants derived from L, b and t.

Results and analysis

Microstructure of the porous HAp

Figure 2 shows Micro-CT images and SEM micrographs of dip-coated (a) and (c), and infiltrated HAp (b) and (d) scaffolds, respectively. Figure 3 shows the microporosity on the surface of a ligament of HAp processed using a foam template with 30% density.

Results of the porosity measurements are depicted in Fig. 4. Analyses using both Micro-CT and SEM images found the porosity of the infiltrated samples to be higher than the original foam template density. This is presumably due to incomplete slip-infiltration and shrinkage during sintering. Nevertheless there is a linear relationship between porosity and preform density for both the infiltration and dip-coating methods. The pore diameter distribution in Fig. 5 shows a broad range for the dip-coated sample and a narrow size distribution for the infiltrated sample. The pore size distribution for infiltrated samples is governed by the ligament diameter of the foam template, which has only a small

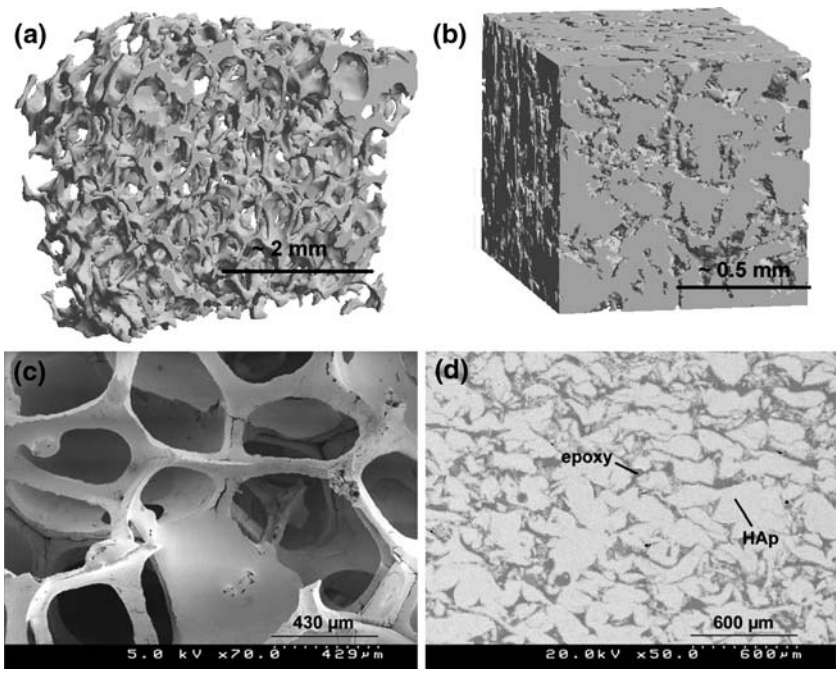

Fig. 2 Porous structures, 3D Micro-CT images of (**a**) dip-coated sample, 2.5 % foam template density, (**b**) infiltrated sample, 30 % foam template density and SEM micrographs of (**c**) dip coated sample, 2.5 % foam template density, (**d**) infiltrated sample, 30 % foam template density, embedded in epoxy resin

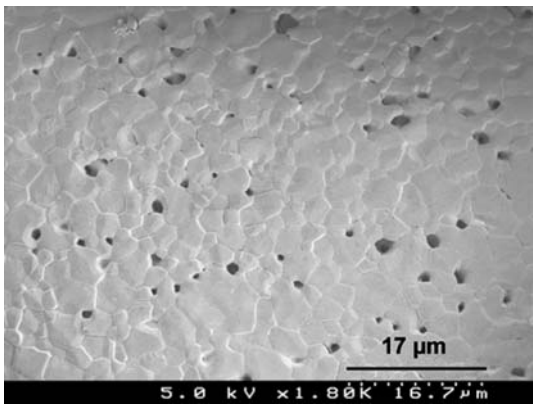

Fig. 3 SEM image of the surface of a HAp ligament, processed from infiltration 30% density foam, showing microporosity

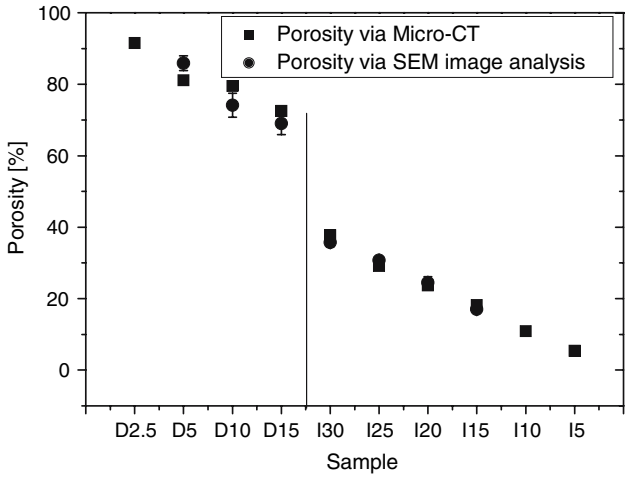

Fig. 4 Macroporosity measured via Micro-CT and SEM image analysis. Letters stand for dip-coated (D) and infiltrated (I) samples, numbers are the polyurethane foam template density in %

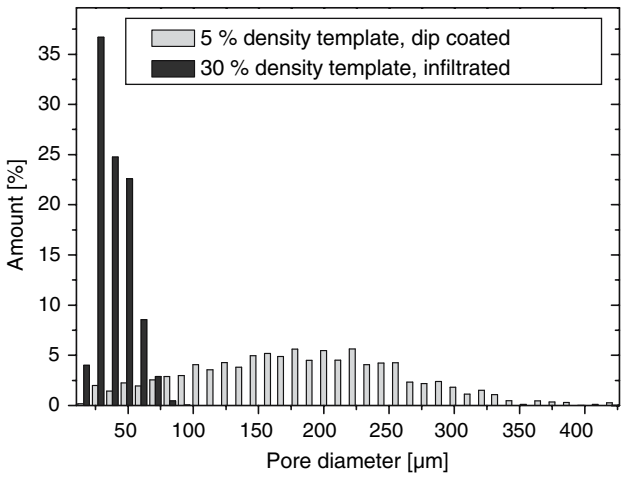

Fig. 5 Pore diameter distributions measured by Micro-CT for an infiltrated sample with 30% foam template density and a dip-coated sample with 5% foam template density

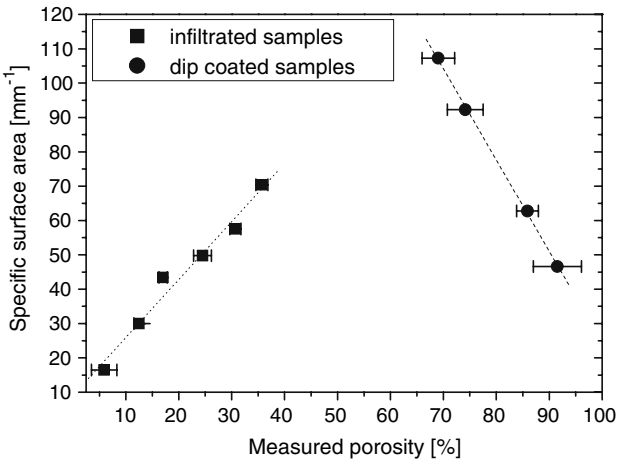

Fig. 6 Specific surface area for infiltrated and dip-coated porous HAp structures

variation. Pores in the dip-coated samples come from both these same ligaments and from the desired incomplete foam infiltration, which leads to a broad distribution of coarser pores. Specific surface area increases for the infiltrated samples and decreases for the dip-coated samples with increasing porosity as can be seen in Fig. 6. The increase for the infiltrated samples is due to additional surfaces created by a higher compression ratio of the foam template, which means an increasing amount of similar-sized pores per unit volume. As the foam compression ratio was lower for the dip-coated samples with increasing porosity, the specific surface area decreases as the amount of pores is reduced although their size increases. Mean pore size as shown in Fig. 7 shows only a slight increase with porosity for the infiltrated sample as the ligament diameter of the foam preform is constant. There is however a significant increase with porosity for the dip-coated sample as voids between former foam ligaments become larger with lower foam compression ratios used for higher porosities. Sintered HAp has a grain size of 3.3 ± 0.3 µm and contains 4.2 ± 0.5% micropores

A graded porous HAp scaffold was successfully produced and a micrograph is shown in Fig. 8. The graph compares the porosity values obtained by area analysis for the graded sample with the standard deviation band of porosity for the ungraded samples as calculated from the SEM and micro-CT images (i.e. data in Fig. 4). It can be seen that the porosity values for the graded samples compare very well with the corresponding ungraded sample except for the dip-coated layer with the highest porosity (derived from the foam template with 5% density). It was noticed that small amounts of the dip-coating slip were drawn from one layer into the layer below. This may explain the higher porosity observed in the 5% layer, as the removed slip cannot be replaced from a layer above.

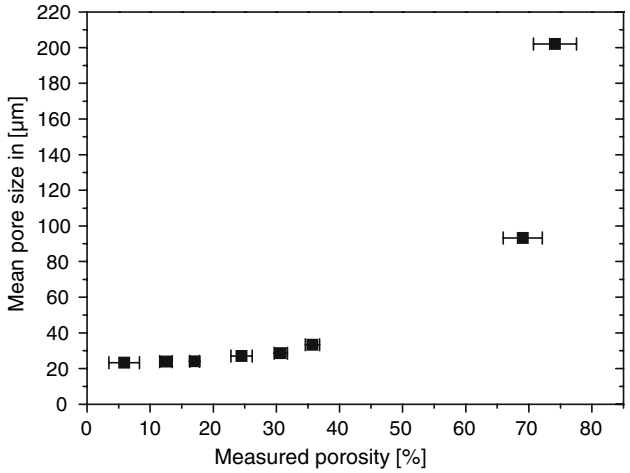

Fig. 7 Mean pore size for porous HAp

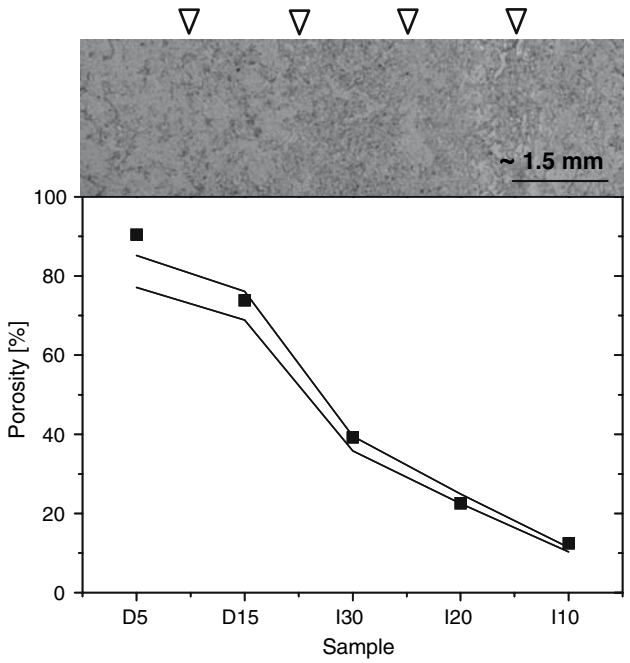

Fig. 8 Light microscopy image of a graded sample with decreasing porosity from left to right. The porosity values in the graph below are obtained via area analysis of the layers. The band is the corresponding standard deviation from area analysis of the ungraded samples as given in Fig. 3

Microstructure of the HAp/$CaCO_3$ composite

After sintering, pure $CaCO_3$ contains 9.2 ± 3.6% microporosity due to incomplete sintering and has a grain size of 2.4 ± 0.4 µm. A linear shrinkage of 15.8 ± 3.8% occurred during sintering of $CaCO_3$. In the composite material even the smallest pore channels of the infiltrated HAp scaffolds were filled with $CaCO_3$ as shown in Fig. 9b. However the shrinkage of the $CaCO_3$ phase has lead to the separation of the HAp/$CaCO_3$ interface in some instances as can be seen in Fig. 9a.

Elastic moduli and compressive strength

Young's, E, and shear, G, moduli for the HAp scaffolds, the HAp/$CaCO_3$ composites, and the dense components for both infiltrated and dip-coated samples are shown in Fig. 10. The values for the porous HAp processed using both techniques, excluding the dense samples, show an exponential decrease with decreasing HAp content [13]:

$$E = E_0 \cdot \exp(-b_E P) \tag{4a}$$

$$G = G_0 \cdot \exp(-b_G P) \tag{4b}$$

There are two types of porosity in the microstructures; macroporosity resulting from the foam template and microporosity within the HAp ligaments. Applying Eq. 4 simultaneously to both samples, E_0 and G_0 are initially taken to represent the moduli of the individual ligaments of the HAp, P is the macroporosity created by the foam template and b_E and b_G are pore geometry factors, both found by regression to be ~0.1. The theoretical elastic moduli of the HAp ligaments can be calculated from the dense samples which were measured to E_0 = 60.9 ± 5.4 GPa and G_0 = 19.9 ± 1.8 GPa, respectively. Noting that the dense HAp has a microporosity of 4.2%, seen within Fig. 3, the theoretical Young's modulus of the HAp ligaments can be estimated, using the same value of b_E = 0.1, to be 92.7 GPa which is in the same range observed by others [14].

Elastic moduli values for the composite material are significantly higher, because the macropores are completely filled with $CaCO_3$. A moderate decrease in modulus can be seen with decreasing HAp content. Below a HAp content of ~80 % the slope of the curve increases due to the effect of porosity created by shrinkage of the $CaCO_3$ within the HAp scaffold during sintering of the $CaCO_3$ and decreased again for the composite created by dip-coating with low HAp contents.

Compression strength σ results are shown in Fig. 11. The data for the porous scaffolds follow an exponential relationship of the form [15]:

$$\sigma = \sigma_0 \cdot \exp(-b_\sigma P) \tag{5}$$

where σ_0 is the theoretical compression strength of the ligaments (224 MPa) calculated from sintered HAp (σ = 160.2 MPa, P = 4.2%), P is the porosity created by the foam template, and b_σ is a pore geometry factor (here found to be 0.08). The compressive strength of the composites can by increased by a factor of 5 compared to porous HAp with a porosity between 20 and 40%, due to the decrease in porosity.

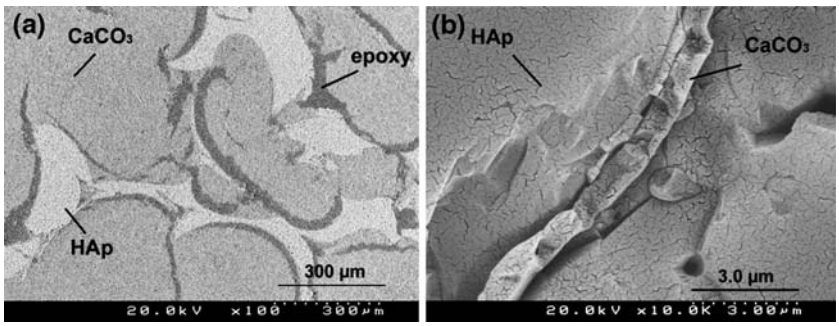

Fig. 9 SEM micrographs of the composite, (**a**) dip coated sample with 5% foam template density, embedded in epoxy resin, (**b**) infiltrated sample with 10% foam template density

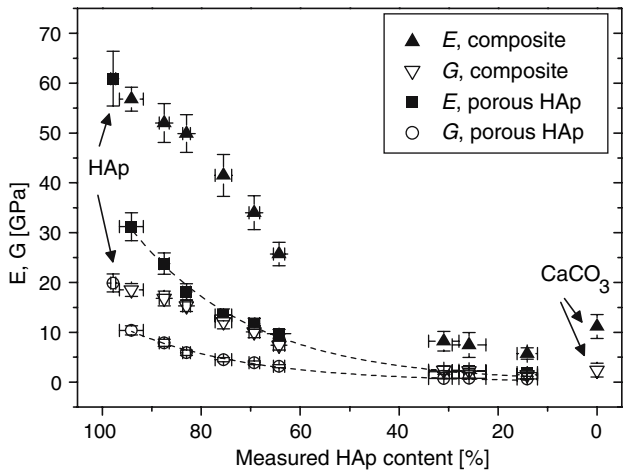

Fig. 10 Young's, E, and shear, G, moduli for dense and porous HAp, the composite material and the dense $CaCO_3$. Dashed lines are fits of Eq. 4

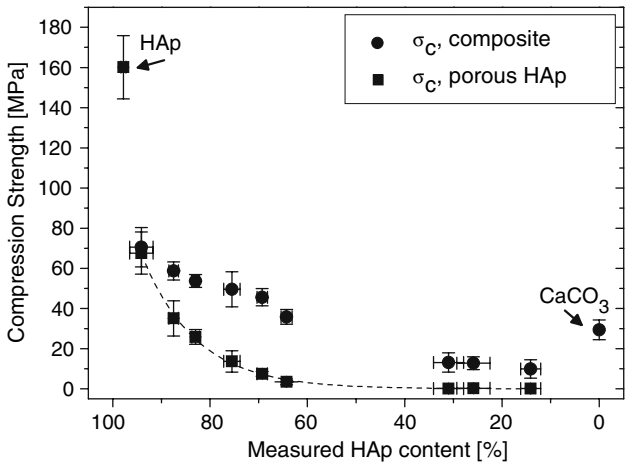

Fig. 11 Compressive strength for dense and porous HAp, the composite material and dense $CaCO_3$. Dashed line is fit of Eq. 5

Discussion

Important requirements for bone-scaffold materials are: interconnected macroporosity suitable for bone ingrowth, satisfactory strength for mechanical integrity to withstand implantation and subsequent loading in service, and appropriate moduli to avoid possible stress-shielding effects. The porous scaffolds developed in this work satisfy all of these requirements. Bioactive but non-bioresorbable scaffolds of hydroxyapatite having designed pore sizes and pore size distributions were developed using infiltration and dip coating techniques. Moreover, combining these techniques enabled porous constructs having graded porosity to be fabricated. It is well demonstrated that bone ingrowth is facilitated by pore diameters in the range of approximately 100–600 µm [16–19]. The porous scaffolds developed in this work contained pores up to typically 400 µm. The dip-coated constructs, in particular, contain pore sizes up to ~400 µm whereas the constructs formed by infiltration contained pores at the lower size limit. As indicated in Fig. 9a, the pores could be filled readily with both the $CaCO_3$ suspension (for the composite scaffold) and with epoxy resin (for microstructural analysis) indicating that the pore network is highly interconnecting. Therefore, it is anticipated that the designed porosity should support the cascade of physiological fluid infiltration, cellular migration, and vascularisation necessary for tissue ingrowth, in particular bone, into the scaffolds.

Almost complete filling of the porosity with $CaCO_3$ significantly increased the compressive strength of the hydroxyapatite scaffolds. This good compressive strength should render the composite structure sufficiently robust for implantation and any reasonable compressive loading encountered during the early stages of service. $CaCO_3$ is a bioresorbable ceramic and it is anticipated that it would be progressively resorbed by bone as part of bone ingrowth into the hydroxyapatite scaffold. Therefore, the initial compressive strength of the scaffold would be maintained to a significant degree, or possibly even increased, as the $CaCO_3$ is replaced by bone tissue. The use of $CaCO_3$ to guide tissue ingrowth has been reported previously [10, 20] but its role in providing increased strength to bioactive ceramic constructs has not been proposed previously. The sintering temperature used for the $CaCO_3$ was limited by the decomposition temperature of the ceramic and was well below that required for appreciable densification and consequently the $CaCO_3$ phase in the macro-pores of the

hydroxyapatite remained relatively porous. It is probable that this would favor physiological resorption of the $CaCO_3$. Furthermore, it is possible that the kinetics of $CaCO_3$ resorption could be modulated by controlling the degree of porosity of the $CaCO_3$ phase through control of the sintering parameters. In particular, it may be possible to match the rate of $CaCO_3$ resorption with that of bone ingrowth into the scaffold such that the mechanical properties of the scaffold are maintained after implantation.

The elastic and shear moduli of the hydroxyapatite scaffolds were significantly increased by the almost complete filling of the porosity with $CaCO_3$. Notably, the moduli are in the range of human bone, which should minimize any stress-shielding effects of the composite scaffold on surrounding bone that could otherwise degrade the long-term bone-implant interface [21]. Combining the dip and infiltration techniques produced a scaffold construct having a graded porosity ranging from ~90 down to ~10% (Fig. 8) with the size of porosity ranging correspondingly from 200 down to 25 μm (Fig. 7). It is anticipated that such a construct is attractive for bone bonding applications because it should permit good bone ingrowth at the high porosity surface and any mechanical loading at the bone-implant would be distributed over the graded section [22]. Furthermore, the latter also would assist in minimizing stress-shielding at the implant-bone interface.

Conclusions

The work presented here has two major outcomes. Firstly, a technique was developed to tailor and control porosity over a broad porosity range in hydroxyapatite. This allows the graded structure to be adapted to suit different purposes. Secondly, the porosity was able to be uniformly filled with an osteoconductive bioresorbable material. It is envisaged that the composite structure will form a useful material for bone replacement applications. The hydroxyapatite will provide immediate bone filling whilst the progressive resorption of $CaCO_3$ will facilitate the ingrowth of bone tissue into the porous structure. The interconnecting porosity should enable physiological fluids to make contact with all areas of the implant whilst the presence of $CaCO_3$ or bone tissue within the porous structure should ensure good mechanical properties of the bone-implant composite [16, 22]. Both properties make this technique promising for a broad range of orthopaedic applications.

Acknowledgements The authors gratefully acknowledge previous work by Achim Neubrand (Fraunhofer-Institut für Werkstoffmechanik, Freiburg, Germany), Matthew Tilbrook and Lyndal Kidson (both former PhD students at the School of Materials Science and Engineering, UNSW) on sponge replica methods for graded alumina. This work provided the basis to develop the porous hydroxyapatite structures described in this paper. The authors also thank Katie Levick and Jenny Norman (both of the Electron Microscope Unit, UNSW) for their many hours spent in optimising the Micro-CT image capturing parameters, which greatly improved the quality of the results. Lastly, the authors thank Viera Piergova (Electron Microscope Unit, UNSW) for the training in SEM use and constant suggestions for improvement of capturing SEM images.

References

1. R. E. HOLMES, R. W. BUCHOLZ and V. MONNEY, *J. Bone Jt. Surg.* **68A** (1986) 904
2. L. L. HENCH, *J. Am. Ceram. Soc.* **74** (1991) 1487
3. F. R. CHICHOCKI, K. P. TRUMBLE and J. RÖDEL, *J. Am. Ceram. Soc.* **81** (1998) 1661
4. W. POMPE, H. WORCH, M. EPPLE et al. *Mat. Sci. Eng. A* **362** (2003) 40
5. R. B. MARTIN, *Materials Science Forum* **293** (1999) 5
6. U. DEISINGER, F. STENZEL and G. ZIEGLER, *Key Eng. Mat.* **264–268** (2004) 2047
7. M. TILBROOK, R. J. MOON and M. HOFFMAN, *Mat. Sci. Eng. A* **393** (2005) 170
8. R. Z. LEGEROS and J. P. LEGEROS, *Key Eng. Mat.* **240–242** (2003) 3
9. F. MONCHAU, A. LEFÈVRE, M. DESCHAMPS et al. *Biomolecular Eng.* **19** (2002) 143
10. K. T. KOO, G. POLOMENI, M. QAHASH et al. *J. Clin. Periodontology* **32** (2005) 104
11. M. F. ASHBY, *Metall. Trans. A*, **14** (1983) 1755
12. ASTM standard C 1259–98
13. R. M. SPRIGGS, *J. Am. Ceram. Soc.* **44** (1961) 628
14. M. A. LOPES, R. F. SILVA, F. J. MONTEIRO and J. D. SANTOS, *Biomaterials* **21** (2000) 749
15. R. W. Rice, Treatise on Materials Science and Technology 11 Properties and Microstructure, edited by R. K. Mac Crone (Academic: New York) p. 191
16. K. A. HING, S. M. BEST and W. BONFIELD, *J. Mater. Sci: Mater. Med.* **10** (1999) 135
17. J. D. BOBYN, R. M. PILLIAR and H. U. CAMERON, *Clin. Orthop. Rel. Res.* **150** (1980) 263
18. F. R. ROSE, L. A. CYSTER, D. M. GRANT et al. *Biomaterials* **25** (2004) 5507
19. H. SCHLIEPHAKE, F. W. NEUKAM and D. KLOSA, *Int. J. Oral Maxillofac. Surg.* **20** (1991) 53
20. K. FUJIHARA, M. KOTAKI and S. RAMAKRISHNA, *Biomaterials* **26** (2005) 4139
21. T. KOKUBO, H. M. KIM and M. KAWASHITA, *Biomaterials* **24** (2003) 2161
22. C. SCHILLER, C. RASCHE and M. WEHMOLLER, *Biomaterials* **25** (2004) 1239